

# Numerical modal analysis of DTU 10-MW reference wind turbine blade using the modified Myklestad's method

L. M. Pereira<sup>a,\*</sup>, M. T. S. Alves<sup>b</sup>

<sup>a</sup>Laboratory of Vibrations and Acoustics, Federal University of Santa Catarina, 88040-900 Florianópolis, Brazil

<sup>b</sup>Laboratory of Computational Mechanics, Polytechnic School, Federal University of Bahia, 40210-630 Salvador, Brazil

Received 10 December 2021; accepted 28 May 2022

---

## Abstract

Since the rotor blade system of an horizontal axis wind turbine is responsible for converting wind energy into mechanical, which turns into electrical and predicting its dynamic behavior is of vital importance. In that sense, this paper deals with performing a modal analysis of a blade belonging to the DTU 10-MW reference wind turbine by using a modified Myklestad's method. The blade model was built on two different keystones, as follows: first, considering uncoupled bending in out-of-plane (flapwise) and in-plane (edgewise) directions and considering a coupled bending-torsion motion also in both directions. In order to accomplish these objectives, a Python code was implemented. The computed eigenfrequencies were compared to the results obtained for the blade by using the finite element method. Besides, the mode shapes were plotted and the centrifugal stiffening was also taken into account. Results suggest the feasibility of the modified Myklestad's method for modal analysis purposes, since good agreement with reference data was achieved and considering that the Myklestad's method has a considerably less complex implementation than the finite element method.

© 2022 University of West Bohemia.

*Keywords:* Myklestad's method, modal analysis, structural dynamics, wind energy

---

## 1. Introduction

As highlighted by [4], the global ambition for increasing renewable share in electric energy production has led to a high demand for wind turbines. This trend is due to the technological solutions that allowed for better generation equipment (wind turbines), for more economically feasible wind farms installations and for the world's commitment on increasing sustainable sources shares in the energy market. According to [12], as the energy demand continuously grows, wind turbine's engineering has evolved over the years to provide more efficient solutions with increased power generation, which implies that wind turbine components have become larger. The large scale of such dynamic mechanical structures is a challenge for engineers that must guarantee their long-life safe operation with the lowest maintenance cost possible as the turbine is submitted to stochastic loads induced by environmental aspects (e.g., turbulences). Because of the tower and the blades slenderness, special attention must be paid to their dynamic behavior and control in order to avoid major aeroelastic instabilities and, thus, failures. Hence, it is important to predict the dynamics of these components in the early design phases. Despite the aeroelastic effects on the wind turbine operation and the key role of the tower in the turbine structural dynamics, this paper focuses on a pure dynamic investigation of a wind turbine blade. When performing dynamic studies of any structure, one of the first steps is to determine the most

---

\*Corresponding author. Tel.: +55 483 721 92 27 (Ext. 200), e-mail: lucas.meirelles@lva.ufsc.br.  
<https://doi.org/10.24132/acm.2022.728>

dominant eigenfrequencies, which are flexural eigenfrequencies when considering wind turbine blades. It turns out that these components are known to have coupled bending-torsion motion due to their structural characteristics, and one should be aware that neglecting such fact is most likely to mislead the results. In this context, [2] arises several techniques to solve this kind of issue, including the Myklestad’s method. Regardless the massive use of the finite element method (FEM) for this purpose, [3, 8] applied a modified Myklestad-Prohl transfer matrix method to perform a modal analysis on a helicopter blade. More recently, [14] used Myklestad approach to predict both eigenfrequencies and mode shapes of a wing and [9] performed a modal numerical analysis of a helicopter blade by using the Holzer-Myklestad method. The purpose of this work is to evaluate the flexural eigenfrequencies and mode shapes of the DTU 10 MW reference wind turbine (RWT) blade, conceived and investigated by [1], in both the flapwise (out-of-plane) and edgewise (in-plane) directions, which can be distinguished as shown in Fig. 1. While the results presented by [1] were obtained by DTU Wind Energy proprietary codes, based on the finite element method, we propose a more computationally affordable approach using an in-house Python code, based on Myklestad’s derived theories.

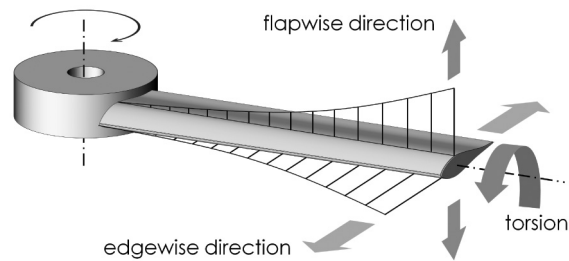


Fig. 1. Blade flexural vibration modes directions

## 2. Theoretical background

The Myklestad’s method for beams is suitable for the solution of flexural systems eigenfrequencies and their respective mode shapes, and it was first presented in [5]. Through this method, a continuous beam is modeled as a discrete system, in which lumped masses are connected by massless sections that account for the structural stiffness. At first, Myklestad’s theory considered static beams with uncoupled bending motion, and one of its main real-world applications was on airplane wings. Later, [6] proposed minor modifications in the former equations to expand the theory application to rotating beams such as propellers and turbine blades, which are subjected to the rotation inertial effect known as centrifugal stiffening. In [10], a polynomial frequency equation method was developed to determine the natural frequencies of a cantilever beam mounted on a rotating disc, based on Myklestad’s expressions. This work brought modified Myklestad’s equations that allowed beams with coupled bending-torsion vibration modes to be modeled. Thus, structures like wind turbine blades that exhibit coupled bending-torsion motion, caused by structural pretwist and asymmetric cross-sections, are more precisely represented. The Myklestad’s method formulations for uncoupled bending motion, detailed in [13], were applied to the DTU 10 MW RWT blade in [11], which brought results for the blade natural frequencies.

### 2.1. Modified Myklestad’s method for coupled bending-torsion motion (CBT model)

This method is applied to discrete cantilever beams represented as lumped masses connected by massless beam sections, that account for bending/torsion stiffness. Its full description is given

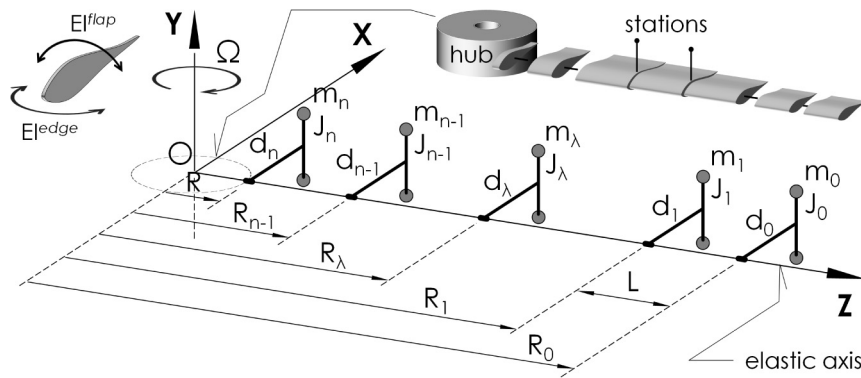


Fig. 2. Blade schematics: (a) typical blade section with its bending stiffnesses, (b) stations locations, (c) rotating asymmetric beam in its undeformed position (adapted from [10])

in [10]. Fig. 2 shows a discrete beam mounted on the periphery of a rotating disc, whose radius is  $R$ . The disc constant angular velocity is  $\Omega$ . The beam has  $n$  stations located at positions  $R_\lambda$ , considering the origin  $O$  at the center of the disc. Every station has its mass  $m_\lambda$  and its inertia  $J_\lambda$ , while  $d_\lambda$  represents the distance between the elastic axis and the station centroid. Each station is apart from each another by a distance  $L$ .

Fig. 3 presents a free body diagram of a section taken from the discrete beam.  $S_\lambda$  is the shear force acting on the  $\lambda$  station,  $M_\lambda$  is the bending moment and  $T_\lambda$  is the torque, which are given as

$$S_\lambda = \omega^2 \sum_{i=0}^{\lambda} m_i (y_i + d_i \theta_i) - \alpha_\lambda \left[ \Omega^2 \sum_{i=0}^{\lambda} m_i R_i \right], \quad (1)$$

$$M_\lambda = \omega^2 \sum_{i=0}^{\lambda-1} m_i (y_i + d_i \theta_i) (R_i - R_\lambda) - \Omega^2 \sum_{i=0}^{\lambda-1} m_i R_i (y_i + d_i \theta_i - y_\lambda - d_\lambda \theta_\lambda) \quad (2)$$

and

$$T_\lambda = \omega^2 \sum_{i=0}^{\lambda} (m_i d_i y_i + J_i \theta_i) - \alpha_\lambda \Omega^2 \sum_{i=0}^{\lambda} m_i R_i d_i, \quad (3)$$

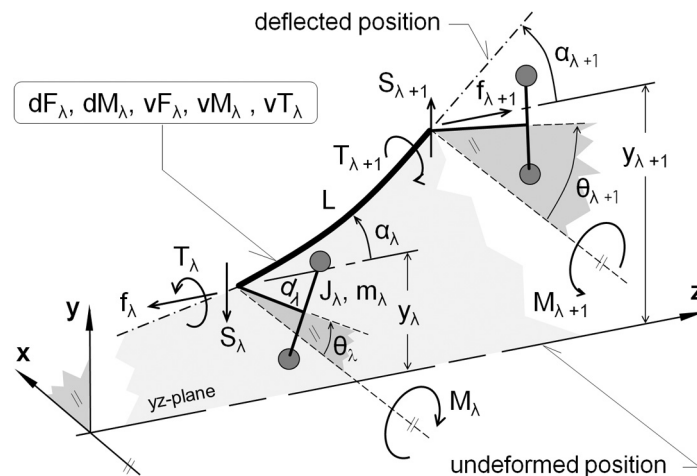


Fig. 3. Free body diagram of an asymmetric beam section in its deflected position (adapted from [13])

respectively. Note that the term between the brackets on the right-hand side of (1) is the contribution from centrifugal force  $f_\lambda$ , since the rotor speed  $\Omega$  is considered (as depicted in Fig. 3).

Additionally, Fig. 3 shows the elastic axis linear deflection  $y_\lambda$ , its slope  $\alpha_\lambda$  and its torsion angle  $\theta_\lambda$ . The massless beam element connecting  $\lambda$  and  $\lambda + 1$  stations accounts for bending and torsion stiffness:  $dF_\lambda = (L^3/3EI)_\lambda$  is the deflection at station  $\lambda$ , relative to station  $\lambda + 1$ , due to a unit force applied at station  $\lambda$ ;  $dM_\lambda = (L^2/2EI)_\lambda$  is the deflection at station  $\lambda$ , relative to station  $\lambda$ , due to a unit moment applied at station  $\lambda + 1$ ;  $vF_\lambda = (L^2/2EI)_\lambda$  is the slope at station  $\lambda$ , relative to station  $\lambda + 1$ , due to a unit force applied at station  $\lambda$ ;  $vM_\lambda = (L/EI)_\lambda$  is the slope at station  $\lambda$ , relative to station  $\lambda + 1$ , due to a unit moment applied at station  $\lambda$ ;  $vT_\lambda = (L/GI_p)_\lambda$  is the torsional deflection at station  $\lambda$ , relative to station  $\lambda + 1$ , due to a unit torque applied at station  $\lambda$ .

It is necessary to express how the parameters from station  $\lambda + 1$  are related to those from station  $\lambda$ . The slope  $\alpha_{\lambda+1}$  can be written as a function of station  $\lambda$  parameters

$$\alpha_{\lambda+1} = \alpha_\lambda - vF_\lambda S_\lambda - vM_\lambda M_\lambda. \tag{4}$$

Similarly, one may find the following for the linear deflection

$$y_{\lambda+1} = y_\lambda - L\alpha_{\lambda+1} S_\lambda - dF_\lambda S_\lambda - dM_\lambda M_\lambda, \tag{5}$$

and for the torsion angle

$$\theta_{\lambda+1} = \theta_\lambda - vT_\lambda T_\lambda. \tag{6}$$

Essentially, this means that every parameter whose index is greater than zero is a function of the values set for station  $\lambda = 0$ .

Since all geometrical parameters (displacement, bending slope and torsion angle) are linearly coupled, the solution for the system eigenfrequencies must consider the linear system

$$\begin{bmatrix} A_1 y_0 & A_2 \alpha_0 & A_3 \theta_0 & \left| & y_n \right. \\ B_1 y_0 & B_2 \alpha_0 & B_3 \theta_0 & \left| & \alpha_n \right. \\ C_1 y_0 & C_2 \alpha_0 & C_3 \theta_0 & \left| & \theta_n \right. \end{bmatrix}. \tag{7}$$

The solving process for the system eigenfrequencies is iterative. Hence, a range of frequencies must be established for a trial and error procedure. For every frequency  $\omega$ , equations (1)–(6) are solved in the presented order, with  $\lambda$  ranging from 0 to  $n$ . The calculations begin by setting boundary conditions for the free-end of the beam, which are  $S_0 = M_0 = T_0 = 0$ . Meanwhile,  $y_0$ ,  $\alpha_0$  and  $\theta_0$  are left to be determined. Initially,  $y_0$  value is set to 1, and  $\alpha_0 = \theta_0 = 0$ . This leads to  $y_n$ ,  $\alpha_n$  and  $\theta_n$  to be constants. Then, computations start over with  $\alpha_0$  left as an unknown quantity, while  $y_0 = \theta_0 = 0$ , which leads to  $y_n$ ,  $\alpha_n$  and  $\theta_n$  to be linear functions of  $\alpha_0$ . Lastly,  $\theta_0$  is left as an unknown quantity, while  $y_0 = \alpha_0 = 0$ , which results in  $y_n$ ,  $\alpha_n$  and  $\theta_n$  being linear functions of  $\theta_0$ . Then, equation (7) is reorganized as follows

$$\begin{bmatrix} 1 & -A_2 \alpha_0 & -A_3 \theta_0 & \left| & A_1 \right. \\ 0 & -B_2 \alpha_0 & -B_3 \theta_0 & \left| & B_1 \right. \\ 0 & -C_2 \alpha_0 & -C_3 \theta_0 & \left| & C_1 \right. \end{bmatrix}. \tag{8}$$

Equation (8) is then solved for  $\alpha_0$  and  $\theta_0$ , which can be replaced in (7) for the solution of  $y_n$ , by considering  $y_0 = 1$ . The resulting value for  $y_n(\omega)$  must be zero, in order to satisfy the boundary conditions for the clamped-end of the beam, for  $\omega$  to be valid as a system eigenfrequency.

## 2.2. Modified Myklestad's method for uncoupled bending motion (UB model)

This approach is similar to the CBT model, but since the UB model does not take torsion motion into account, some modifications are made to the presented equations, which make the solution of the problem simpler. Equations (3) and (6) are not considered. Equations (4) and (5) remain unchanged. All terms regarding distance  $d$  and torsion angle  $\theta$  are removed from (1) and (2), which are then presented as

$$S_\lambda = \omega^2 \sum_{i=0}^{\lambda} m_i y_i - \alpha_\lambda \Omega^2 \sum_{i=0}^{\lambda} m_i R_i \quad (9)$$

and

$$M_\lambda = \omega^2 \sum_{i=0}^{\lambda-1} m_i y_i (R_i - R_\lambda) - \Omega^2 \sum_{i=0}^{\lambda-1} m_i R_i (y_i - y_\lambda), \quad (10)$$

respectively. In this case, the solution for the system eigenfrequencies considers only two variables ( $y_0$  and  $\alpha_0$ ), as in

$$\begin{bmatrix} A_4 y_0 & A_5 \alpha_0 \\ B_4 y_0 & B_5 \alpha_0 \end{bmatrix} \begin{bmatrix} y_n \\ \alpha_n \end{bmatrix}. \quad (11)$$

The trial and error procedure for the frequency range is performed for the UB model, as well. However, only two sets of computations are necessary: the first one with  $y_0 = 1$  and  $\alpha_0 = 0$  and the second one with  $y_0 = 1$  and  $\alpha_0$  left as an unknown quantity. As the boundary condition demands,  $\alpha_n$  must be zero. Hence,  $\alpha_0$  is easily obtained as  $\alpha_0 = -(B_4/B_5)$  and substituted into (11) for  $y_n$ . Here, once again, the valid system eigenfrequencies are the roots of the polynomial  $y_n(\omega)$ . More details regarding these methods can be found in [6, 10, 13].

## 3. Methodology

The DTU 10 MW RWT blade is about 90 meters long and weighs approximately 41 tons [1]. The aforementioned formulations were coded and validated as per numerical example, given in [10]. The code was then applied to the DTU 10 MW RWT blade, whose structural parameters are available in [1] for 51 cross sections along the blade length, as follows: radial position  $r$  [m], mass per unit length  $m_L$  [kg/m], flapwise bending stiffness  $EI^{flap}$  [N m<sup>2</sup>], edgewise bending stiffness  $EI^{edge}$  [N m<sup>2</sup>], torsional stiffness  $GI_p$  [N m<sup>2</sup>], radius of gyration about flapwise axis  $R_{gyr}^{flap}$  [m], and radius of gyration about edgewise axis  $R_{gyr}^{edge}$  [m]. From these parameters, one can obtain the radius of gyration about the  $z$  axis as follows

$$R_{gyr}^z = \sqrt{\left(R_{gyr}^{flap}\right)^2 + \left(R_{gyr}^{edge}\right)^2}. \quad (12)$$

The center of the hub was set as the origin of the reference frame, as shown in Fig. 4.

The blade flapwise and edgewise eigenfrequencies were assessed by means of the CBT and UB formulations presented in Sections 2.1 and 2.2, respectively, with different levels of discretization:  $n = 50, 250$  and  $1000$  stations, where  $n$  is the number of stations.

The processing time was measured for both formulations, which ran in a system powered by Intel© i5-7200U processor (2.5 GHz) and 8 GB RAM. For the CBT results, the blade mode shapes are presented and the effects of centrifugal stiffening on the eigenfrequencies are evaluated within a range of rotor speeds that include the RWT operational limits (from 6.0 to 9.6 rpm). In this work and for the reader's convenience, it should be pointed out that some

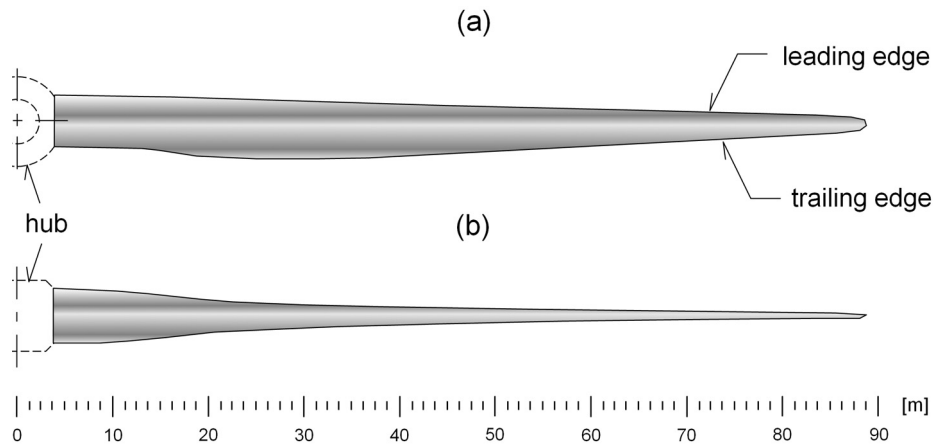


Fig. 4. DTU 10 MW RWT blade: (a) top view (XZ-plane), (b) front view (YZ-plane) (adapted from [7])

key assumptions were made resulting from the application of the Myklestad's method. These assumption are listed as follows:

- (i) All formulations are derived assuming a unidimensional modeling, i.e., the blade is a discretized line with area properties attached to each station.
- (ii) Apart from cross-sections locations, cords and thicknesses, no CAD files were evaluated.
- (iii) The elastic axis of the blade is considered colinear, and its deflection occurs either in the XZ- or YZ-plane.
- (iv) The structural twist angle between the blade's cross-sections was not taken into account, so the sections principal axis was treated as aligned to the reference frame.
- (v) The cross-section mass is uniformly distributed, so the center of mass is coincident with the cross-section centroid.
- (vi) The distance between the elastic axis and the station centroid  $d$  was considered equal to the corresponding cross section  $R_{gyr}^z$ , which is given by (12).

#### 4. Results and discussions

The aim of this section is to present the eigenfrequencies obtained by both the UB and CBT models, as well as the mode shapes extracted from the CBT model ( $n = 1\ 000$ ) and the effects of the centrifugal stiffening on the eigenfrequencies of the blade, also evaluated for the CBT model ( $n = 1\ 000$ ).

##### 4.1. Blade eigenfrequencies

Table 1 provides a comparison between the UB and CBT performances with the reference values (BAK) given in [1] for the flapwise direction. By contrast, Table 2 is dedicated to the comparison of edgewise direction results.

At first glance, it becomes apparent that the CBT model performed better than the UB model in terms of results accuracy, once the frequencies estimated from the CBT model converged to values closer to the reference ones provided in [1]. In general, flapwise modes demonstrated to be less sensitive than edgewise modes to the assumptions on which the models were based on. The processing time for the CBT models were about three times greater than for the UB models, which can be attributed to the larger number of variables and equations complexity of

Table 1. Comparison between flexural eigenfrequencies of the DTU 10 MW RWT blade obtained by the UB and CBT models – **flapwise direction (out-of-plane)**

<i>n</i>	mode	eigenfrequency [Hz]			deviation [%]		processing time [s]	
		BAK	UB	CBT	UB/BAK	CBT/BAK	UB	CBT
50	1	0.61	0.59	0.59	−3.28	−3.28	1.83	4.56
	2	1.74	1.70	1.68	−2.30	−3.45		
	3	3.57	3.52	3.42	−1.40	−4.20		
	4	6.11	6.00	5.72	−1.80	−6.32		
250	1	0.61	0.61	0.61	0.00	0.00	8.59	22.50
	2	1.74	1.76	1.73	1.15	−0.57		
	3	3.57	3.65	3.54	2.24	−0.84		
	4	6.11	6.24	5.94	2.13	−2.78		
1 000	1	0.61	0.62	0.62	1.64	1.64	37.33	99.27
	2	1.74	1.77	1.74	1.72	0.00		
	3	3.57	3.68	3.57	3.08	0.00		
	4	6.11	6.31	6.01	3.27	−1.64		

Table 2. Comparison between flexural eigenfrequencies of the DTU 10 MW RWT blade obtained from the UB and CBT models – **edgewise direction (in-plane)**

<i>n</i>	mode	eigenfrequency [Hz]			deviation [%]		processing time [s]	
		BAK	UB	CBT	UB/BAK	CBT/BAK	UB	CBT
50	1	0.93	0.95	0.94	2.15	1.08	1.83	4.56
	2	2.76	2.85	2.74	3.26	−0.72		
	3	6.66	6.11	5.65	−8.26	−15.17		
250	1	0.93	0.97	0.96	4.30	3.23	8.59	22.50
	2	2.76	2.92	2.81	5.80	1.81		
	3	6.66	6.26	5.79	−6.01	−13.06		
1 000	1	0.93	0.97	0.96	4.30	3.23	37.33	99.27
	2	2.76	2.94	2.83	6.52	2.54		
	3	6.66	6.31	5.83	−5.26	−12.46		

the coupled bending-torsion formulations. Since [1] presented no processing information (such as computational setup and processing time), it was not possible to compare the computational performance of the UB and CBT models with the results obtained by the FEM algorithm. For the flapwise modes, the UB model converged to overestimated values of the eigenfrequencies. The first mode was relatively well predicted with an absolute deviation of only 0.01 Hz (or 1.64%), but as for the higher modes, larger errors were verified, as observed for the fourth eigenfrequency, which exhibited a 3.27% deviation from the reference value. On the other hand, the CBT model predicted exactly the second and third flapwise eigenfrequencies, while the first mode was overestimated by the same amount of UB’s prediction and the fourth mode was underestimated by −0.10 Hz (or −1.64%).

As for the edgewise modes, greater deviations were found. Surprisingly, both methods achieved better agreement with [1] when coarser discretizations were applied and increased the deviation when greater numbers of stations were considered. The only exception is the third mode, whose deviation drops with finer discretizations, but still exhibits significant outlier results. Given this anomalous behavior, the authors’ hypothesis is that this gap has to do with the simplifying assumptions made in the methodology, since other results revealed good agreement, especially those obtained by using the CBT approach. Disregarding the third mode, the UB model predicted edgewise natural frequencies with a maximum deviation of 6.52%, while the CBT model presented a maximum deviation of 3.23%.

**4.2. Blade mode shapes**

The blade flapwise mode shapes occur by the movement of the elastic axis along the YZ-plane that is the direction normal to the rotation plane. Figs. 5–8 depict the flapwise mode shapes computed for the RWT blade by the CBT model considering the finest discretization ( $n = 1\,000$ ). Figs. 5(a)–8(a) show the Z-displacement (in the YZ-plane) of the leading edge (LE) and trailing edge (TE) along the blade span, normalized by the tip displacement. It is noticeable that the two curves diverge at some points due to the bending-torsion coupling effect. Figs. 5(b)–8(b) represent the edges movement in the XZ-plane, to improve the torsion effect visualization. All the plotted mode shapes are delimited by an undeformed blade contour (black thinner line). It is possible to visualize the torsion angle effect, especially for the third and fourth modes. All the flapwise modes are also presented in perspective in Fig. 9.

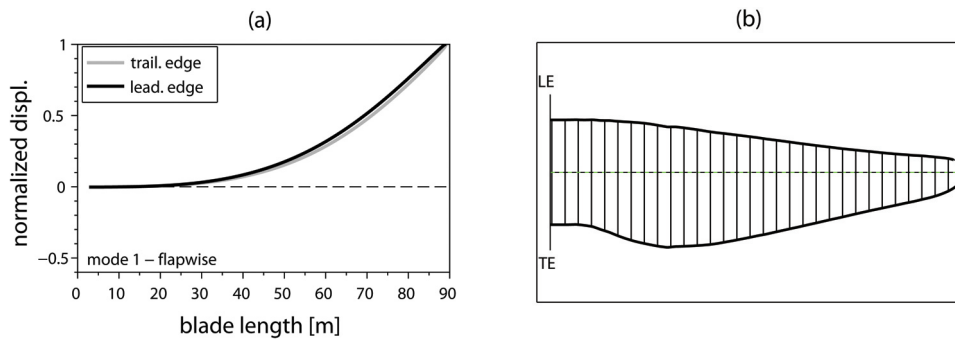


Fig. 5. FLAPWISE – First mode: (a) leading and trailing edges deflections (YZ-plane), (b) top view (XZ-plane)

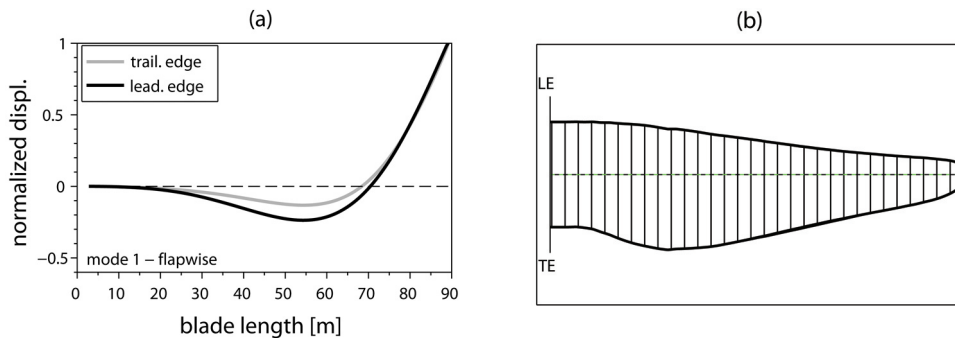


Fig. 6. FLAPWISE – Second mode: (a) leading and trailing edges deflections (YZ-plane), (b) top view (XZ-plane)

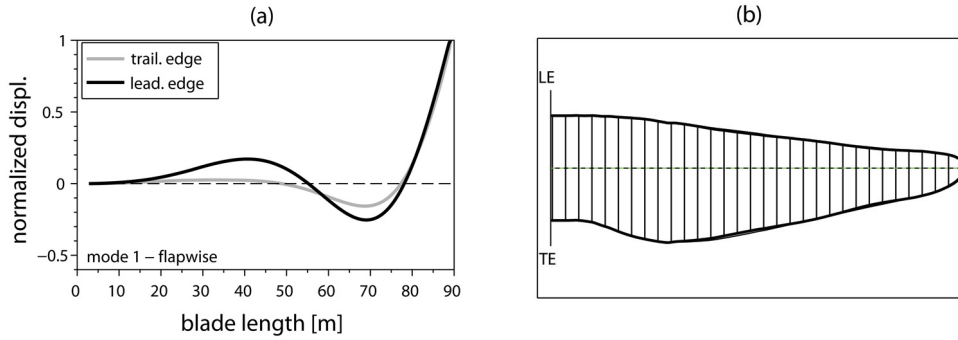


Fig. 7. FLAPWISE – Third mode: (a) leading and trailing edges deflections (YZ-plane), (b) top view (XZ-plane)

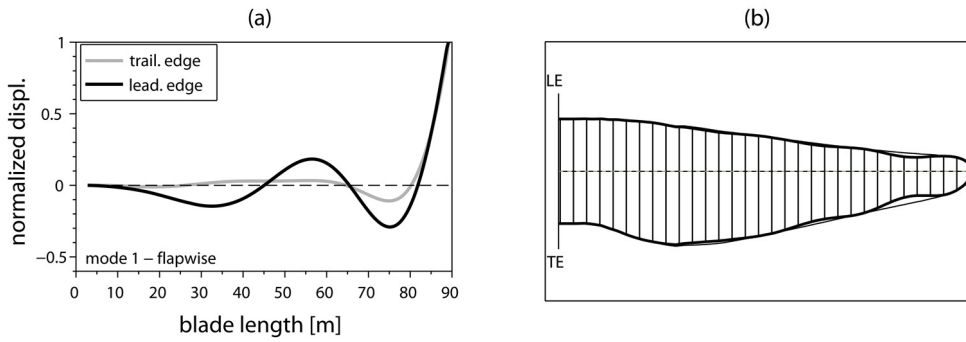


Fig. 8. FLAPWISE – Fourth mode: (a) leading and trailing edges deflections (YZ-plane), (b) top view (XZ-plane)

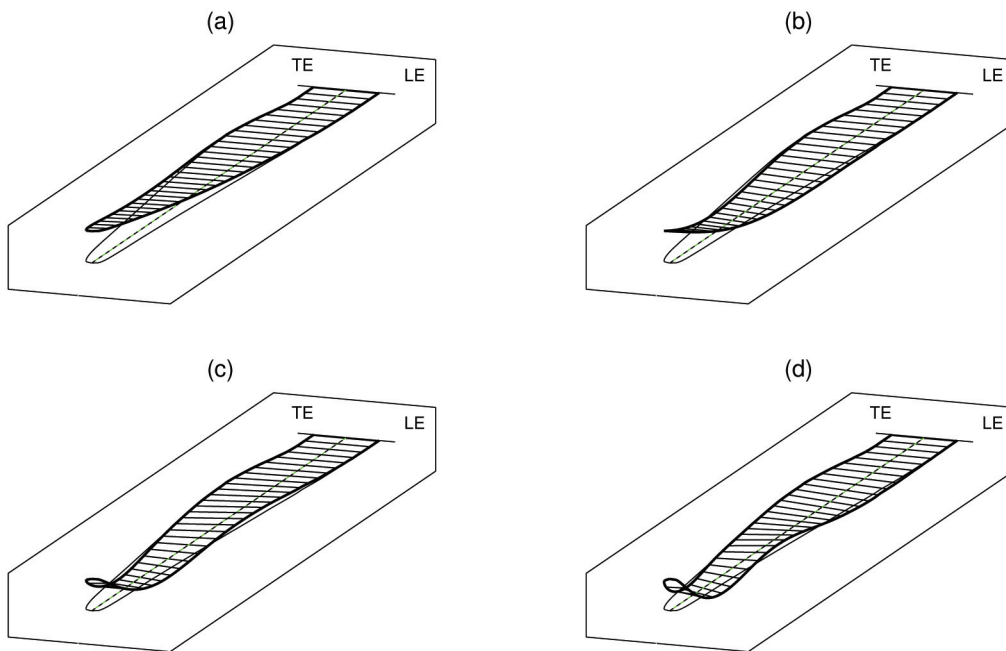


Fig. 9. FLAPWISE modes (perspective): (a) first mode, (b) second mode, (c) third mode, (d) fourth mode

The blade edgewise mode shapes occur by the movement of the elastic axis along the XZ-plane, i.e., the rotation plane. Figs. 10–12 exhibit the edgewise mode shapes also computed by the CBT model with  $n = 1000$ . Once again, Figs. 10(a)–12(a) present the normalized Z-displacement (in the YZ-plane) of the leading edge (LE) and trailing edge (TE) along the blade span. In this case, the results show a more evident torsion effect, as seen by the differences between the LE and TE displacements. Figs. 10(b)–12(b) represent the edges movement in the XZ-plane for the three edgewise modes considered. It is worth to mention that due to the larger bending stiffness in the edgewise direction ( $EI^{edge} > EI^{flap}$ ), the actual bending deflections (non-normalized) expected in the flapwise modes are larger than in the case of the edgewise ones.

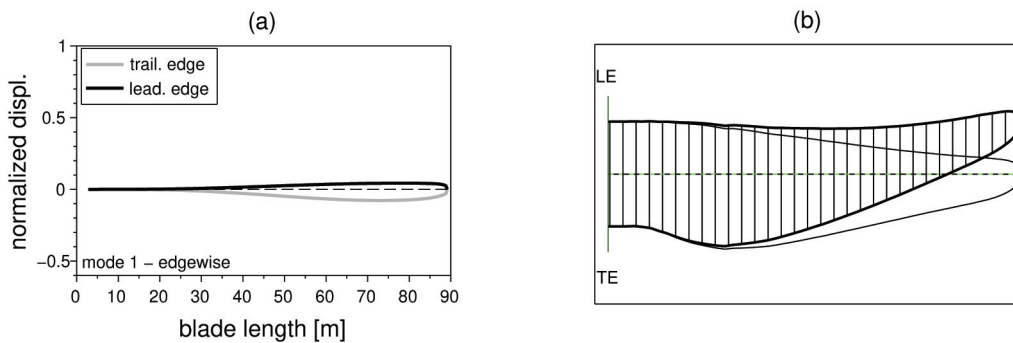


Fig. 10. EDGEWISE – First mode: (a) leading and trailing edges deflections (YZ-plane), (b) top view (XZ-plane)

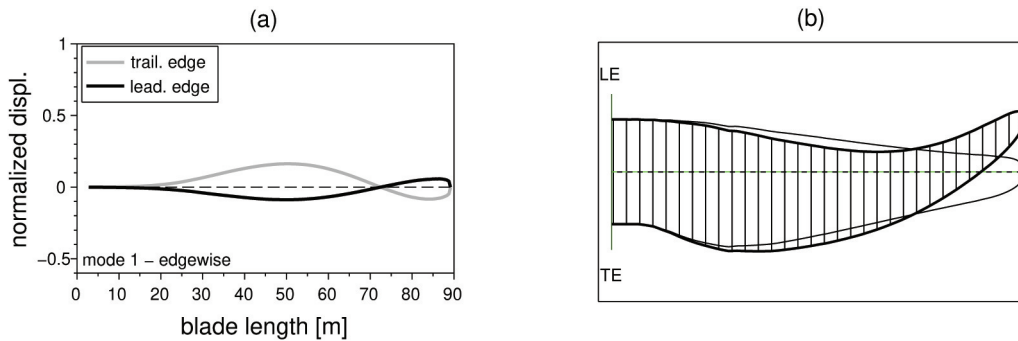


Fig. 11. EDGEWISE – Second mode: (a) leading and trailing edges deflections (YZ-plane), (b) top view (XZ-plane)

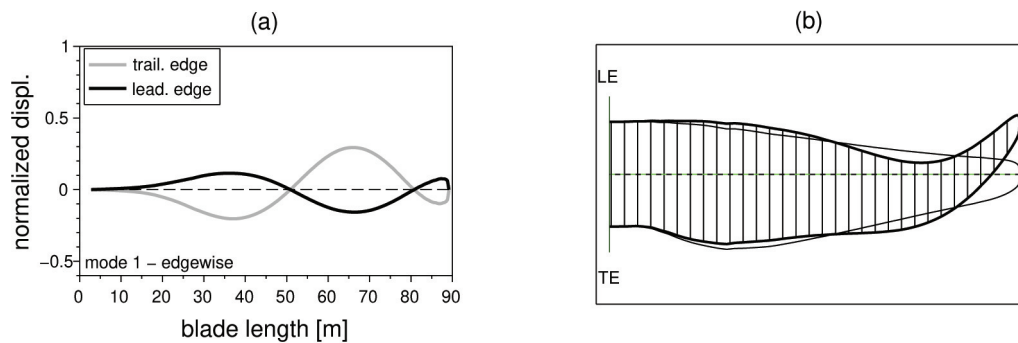


Fig. 12. EDGEWISE – Third mode: (a) leading and trailing edges deflections (YZ-plane), (b) top view (XZ-plane)

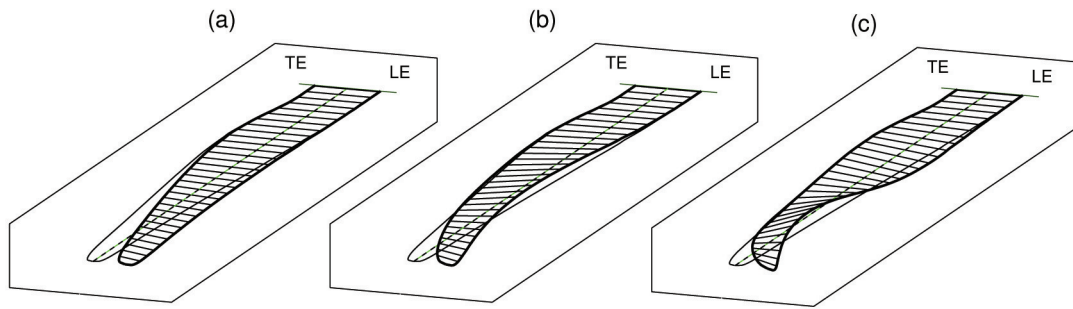


Fig. 13. EDGEWISE modes (perspective): (a) first mode, (b) second mode, (c) third mode

A better visualization of the edgewise modes can be seen in perspective, as shown in Fig. 13.

### 4.3. Centrifugal stiffening

Due to the operation of the wind turbine, each blade behaves as a rotary wing. For this reason, the effect of the centrifugal stiffening should be considered in order to estimate the actual eigenfrequencies and mode shapes during the rotor’s rotation. Thus, based on the finest discretization, the centrifugal stiffening was taken into account within the CBT model. Both Table 3 and Fig. 14 present the eigenfrequencies trend with respect to the rotor speed.

Table 3. Evaluation of the centrifugal stiffening on the blade eigenfrequencies – CBT model ( $n = 1000$ )

rotor speed		eigenfrequencies [Hz]						
		flapwise modes				edgewise modes		
[rpm]	[Hz]	1	2	3	4	1	2	3
0.0	0.00	0.62	1.74	3.57	6.01	0.96	2.83	5.83
6.0	0.10	0.63	1.76	3.58	6.02	0.97	2.84	5.84
9.6	0.16	0.65	1.78	3.61	6.04	0.98	2.85	5.85
60.0	1.00	1.41	2.90	4.86	7.36	1.55	3.59	6.61
96.0	1.60	2.05	4.04	6.33	9.05	2.12	4.50	7.66

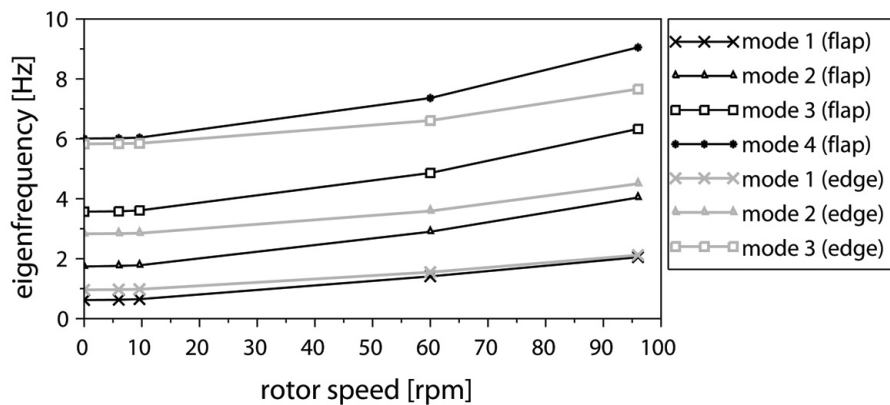


Fig. 14. Centrifugal stiffening effect (Campbell Diagram)

As the limit for operational rotor speed is 9.6 rpm (or 0.16 Hz), the eigenfrequencies exhibit very low sensitivity to the increase in rotor speed in this range, as can be observed in Fig. 14. Aeroelastic and gravity effects were not taken into account in this work.

## **5. Concluding remarks**

The purpose of this work was to evaluate the flapwise and edgewise flexural eigenfrequencies and mode shapes of the DTU 10 MW reference wind turbine (RWT) blade. It was shown that the modified Myklestad's method is suitable for performing modal analysis. The UB model considered uncoupled bending along flapwise and edgewise directions of the blade and the CBT model took the coupling bending-torsion motion into account. All eigenfrequencies were compared in a tabular fashion with the reference data provided for the reference wind turbine. Reasonable agreement was found, even in cases of coarser discretization. All the respective mode shapes obtained by the CBT model were plotted, revealing the torsion effect. Finally, the centrifugal stiffening effect on the eigenfrequencies was evaluated in the case of increasing rotor speed. Based only on the operational speed range, no significant impact was revealed. The results obtained are encouraging in the sense that the Myklestad's method is able to provide reliable baselines if compared with FEM results [1]. Moreover, the models were built under several assumptions. Therefore, despite FEM playing more reliable and robust role from the view point of current industrial applications, the authors consider the investigated method to be an affordable alternative tool for preliminary numerical modal analyses, due to its simpler computational implementation in comparison to FEM.

## **Acknowledgements**

The authors would like to thank the support from Laboratory of Computational Mechanics (LabMeC) under Department of Mechanical Engineering at Polytechnic School/EPUFBA, as well as the contribution from Prof. Guilherme Begnini and Prof. Bruno Diniz as examiners of L. M. Pereira's work, whose results led to the present article.

## **References**

- [1] Bak, C., Zahle, F., Bitsche, R., Kim, T., Yde, A., Henriksen, L.C., Hansen, M.H., Blasques, J.P.A.A., Gaunaa, M., Natarajan, A., The DTU 10-MW reference wind turbine, Technical Report 1, Danmarks Tekniske Univesitet, Lyngby, 2013.
- [2] Bazoune, A., Survey on modal frequencies of centrifugally stiffened beams, *The Shock and Vibration Digest* 37 (6) (2005) 449–469. <https://doi.org/10.1177/0583102405056752>
- [3] Cuesta, J.D., Modeling helicopter blade dynamics using a modified Myklestad-Prohl transfer matrix method, Master's thesis, U.S. Naval Postgraduate School, Monterey-CA, 1994.
- [4] Krog Kruse, E., Sørensen, N.N., Bak, C., A two-dimensional quantitative parametric investigation of simplified surface imperfections on the aerodynamic characteristics of a NACA 633-418 airfoil, *Wind Energy* 24 (4) (2021) 310–322. <https://doi.org/10.1002/we.2573>
- [5] Myklestad, N.O., A new method of calculating natural modes of uncoupled bending vibration of airplane wings and other types of beams, *Journal of the Aeronautical Sciences (Institute of the Aeronautical Sciences)* 11 (8) (1944) 153–162. <https://doi.org/10.2514/8.11116>
- [6] Myklestad, N.O., *Fundamentals of vibration analysis*, New York, McGraw-Hill, 1956.
- [7] Ostachowicz, W., McCugan, M., Schröder-Hinrichs, J.U., Luczak, M., *MARE-WINT: New materials and reliability in offshore wind turbine technology*, Switzerland, Springer Open, 2016. <https://doi.org/10.1007/978-3-319-39095-6>

- [8] Oztruk, D., Development of a Myklestad's rotor blade dynamic analysis code for application to JANRAD, Master's thesis, U.S. Naval Postgraduate School, Monterey-CA, 2002.
- [9] Rabiei, H., Galehrdari, S. A., Modal numerical analysis of helicopter rotor sample using Holzer-Myklestad method, *Journal of Stress Analysis* 3 (1) (2018) 111–121.
- [10] Rao, J. S., Banerjee, S., Coupled bending-torsional vibration of rotating cantilever blades: Method of polynomial frequency equation, *Mechanism and Machine Theory* 12 (1977) 271–280. [https://doi.org/10.1016/0094-114X\(77\)90003-9](https://doi.org/10.1016/0094-114X(77)90003-9)
- [11] Santos, J. P. T. P., Pereira, L. M., Alves, M. T. S., Begnini, G. R., Comparison between finite element method and Myklestad's method to identify the blade flexural natural frequencies of the DTU 10-MW reference wind turbine, *Proceedings of XXIII Encontro Nacional de Modelagem Computacional*, Palmas, Federal University of Tocantins, 2020, pp. 1966–1974.
- [12] van der Tempel, J., Molenaar, D. P., Wind turbine structural dynamics – A review of the principles for modern power generation, onshore and offshore, *Wind Engineering* 26 (4) (2002) 211–222. <https://doi.org/10.1260/030952402321039412>
- [13] Thomson, W. T., *Theory of vibration with applications*, 4th edition, Springer, 1996.
- [14] Yass, M. A. R., Prediction of natural frequency and modes shape of wing using Myklestad method, *Journal of University of Babylon for Engineering Sciences* 26 (6) (2018) 348–361.